AGU **ADVANCING EARTH AND SPACE SCIENCE**

Geophysical Research Letters

Key Points:
- A numerical model is applied to trace the evolving distribution of components over the Chang'e-5 landing region
- The local mare component should account for ~60% in the samples
- The samples could contain abundant Imbrium melt

Predicted Sources of Samples Returned From Chang'e−5 Landing Region

Tiantian Liu[1] [iD], Greg Michael[2] [iD], Meng-Hua Zhu[3] [iD], and Kai Wünnemann[1,2]

[1]Museum für Naturkunde, Leibniz Institute for Evolution and Biodiversity Science, Berlin, Germany, [2]Freie Universität Berlin, Berlin, Germany, [3]State Key Laboratory of Lunar and Planetary Sciences, Macau University of Science and Technology, Taipa, Macau

Abstract China's Chang'e-5 (CE-5) has returned 1.731 kg lunar samples from a young mare unit on December 2020. Here, the authors used a spatially resolved numerical model, which considers both impact mixing and volcanic effusion, to estimate the evolving distribution of components over the landing region. Using this model, the age composition of surface scooped and sub-surface drilled CE-5 samples and their sources were traced back. The proposed model predicts that local mare material predominates in both surface and sub-surface samples and the nonlocal mare component is ~1%. There is ~40% of nonmare component. The composition of both nonmare components in the surface and sub-surface samples are similar: Abundant components are basin-sourced melts, where the Imbrium melt are ~ 25% among all the melt. The ejecta of Sharp B, Harding, Copernicus, and Aristarchus crater that possess different compositions of basin-sourced melt may have significantly altered the material composition of the landing surface.

Plain Language Summary Lunar samples provide the ground-truth reference to reveal the Moon's evolutional history. China's Chang'e-5 mission is the first lunar exploration program that returned samples since the Luna 24 mission in 1976. Although the sampling site is a young mare basalt, the long-term impact gardening and multiple volcanic episodes make the composition of the surface material complicated, impeding the interpretation of samples. Here, the authors conduct a numerical simulation that can trace the evolving distribution of different components on the Moon to predict the material composition on the CE-5 landing region. We found that the local mare material should predominate in both the surface and sub-surface samples (accounting for 60%). We expect ~40% nonmare component. The nonmare component should contain abundant impact-produced melt from the South Pole-Aitken, Serenitatis, and Imbrium basin. Besides, at the CE-5 sampling site, the mixture of ejecta from Sharp B, Harding, Copernicus, and Aristarchus crater that have different compositions of basin-sourced melt cannot be neglected. These predictions can provide useful information for analyzing the provenance of the CE-5 samples.

1. Introduction

The Moon is the only body in space for which we have samples with known locations. The samples provide ground-truth references for our knowledge of lunar origin and evolution (Hiesinger & Head, 2006). China's Chang'e-5 (CE-5) mission, the first lunar sample return mission since Luna 24 in 1976 (Zou & Li, 2017), launched on November 23, 2020. The lander successfully touched down in the Rümker region in northern Oceanus Procellarum (51.8°W, 43.1°N). The return capsule brought back 1.731 kg lunar samples consisting of surface materials collected by a mechanical scoop and subsurface materials contained in the drilling core.

After the formation of the lunar crust, the impact cratering and volcanic mare filling are major processes that alter the composition of surface material. The mare filling process produced mare components inside the basins and the impact cratering process constantly mix the mare/nonmare components. Consequently, the surface where the regolith samples were collected consists of components of various sources (Vaniman et al., 1991). Some components are materials excavated from beneath the surface stratum by local impacts; some components could be the ejecta of impact craters occurred near the sampling site (Beaty & Albee, 1978; Fernandes et al., 2013; Korotev & Jolliff, 2001; Norman et al., 2016; Norman & Nemchin, 2014; Rhodes et al., 1974; Spudis & Ryder, 1981; Wilhelms, 1987). The admixed ejecta from distant

craters represent materials from areas far from the landing site, which remain unexplored. The various components contained in the samples provide selenologic knowledge on the bombardment and volcanic history at the landing region. For the samples collected on the maria, differently aged mare material from the surface near the landing site could be transported by impact to the sampling site, which may allow for unveiling the volcanic history surrounding the landing region. In addition, impact melt of early giant basins (Bottke & Norman, 2017; Petro & Pieters, 2008; Stöffler, 2006; Wilhelms, 1987) could be transported to the landing region, where it was initially buried by subsequently deposited young mare basalts, but was later excavated to the surface by the local impacts. All these processes alter the composition of surface material and the complexity of material composition increases with the cumulative impact mixing. The provenance of different components of material collected at the surface becomes uncertain making the sample interpretation difficult (Vaniman et al., 1991).

Here, we applied a spatially resolved numerical model that considers both impact mixing and mare filling to trace the evolving distribution of mare/nonmare components and to estimate the abundance of different components in the CE-5 samples and their plausible origin (local or exotic; basin or nonbasin). In Section 2, we summarized the major geologic characteristics of the landing region that are considered in the model. The model mechanism is described in Section 3. We then analyzed the material composition over the landing surface (Section 4) and tried to address several key questions for the collected CE-5 samples: What is the main difference of the bulk composition for the samples collected from the surface and the sub-surface? How many separate mare emplacement events are recognizable in the samples? Do any nonmare components in the regolith relate to basins and what is their provenance?

2. Important Geologic Features of the Landing Region for Modeling

The geologic features of the landing region (51–63°W, 41–45°N, Figure 1a) were extensively studied before the launch of the CE-5 spacecraft (e.g., Qian et al., 2018; Wu et al., 2018; Zhao et al., 2017). The features that are closely related to our model are summarized here.

Qian et al. (2018) proposed the chronology and sequence of volcanic activities at the landing site: the earliest detectable volcanism in the landing area erupted around 3.72 Ga ago (Hiesinger et al., 2003), and the volcanism was active until 3.51 Ga ago, forming units Ir1 (3.71 Ga), Ir2 (3.58 Ga), and Ir3 (3.51 Ga) in Mons Rümker (Figure 1b). During the Late Imbrian Period, three major phases of volcanism occurred followed by four major phases of Eratosthenian volcanism. Two of the Imbrian-aged (Im1, 3.42 Ga; Im2, 3.39 Ga) and three of Eratosthenian-aged (Em1, 2.30 Ga; Em3, 1.51 Ga; Em4, 1.21 Ga) mare deposits are located within the landing region. The Eratosthenian mare units are estimated to be ~100 m in thickness, which are thinner than the older Ir-aged and Imbrian-aged units (~700 m).

Most of impact craters inside the landing region are smaller than 2 km in diameter (see Table S3). The distal ejecta of larger craters, which are evident from the ubiquitous occurrence of impact rays, may transport components from afar to the landing surface. These distal ejecta from craters over the Moon, which are younger than the landing region, was thought to contribute ~90% of the total ejecta at the landing area (e.g., Xie et al., 2020). These craters were thus regarded to have transported a nonnegligible volume of their ejecta to the landing area (Figure 1a and Table S1).

3. Model

To trace the evolving distribution of different components for the landing region, both the process of impact mixing and volcanic effusion should be considered. Note that the formations of rilles, vents, domes, and regolith agglutination do not significantly affect the compositions at the landing region; therefore they are not included in our model.

3.1. Cumulative Impact Mixing

In the previous work (Liu, Michael, Wünnemann, et al., 2020), a spatially resolved numerical model was developed to investigate the evolving distribution of different components through long-term impact mixing over the global surface. With the knowledge of lunar chronology and production functions (Neukum, 1983),
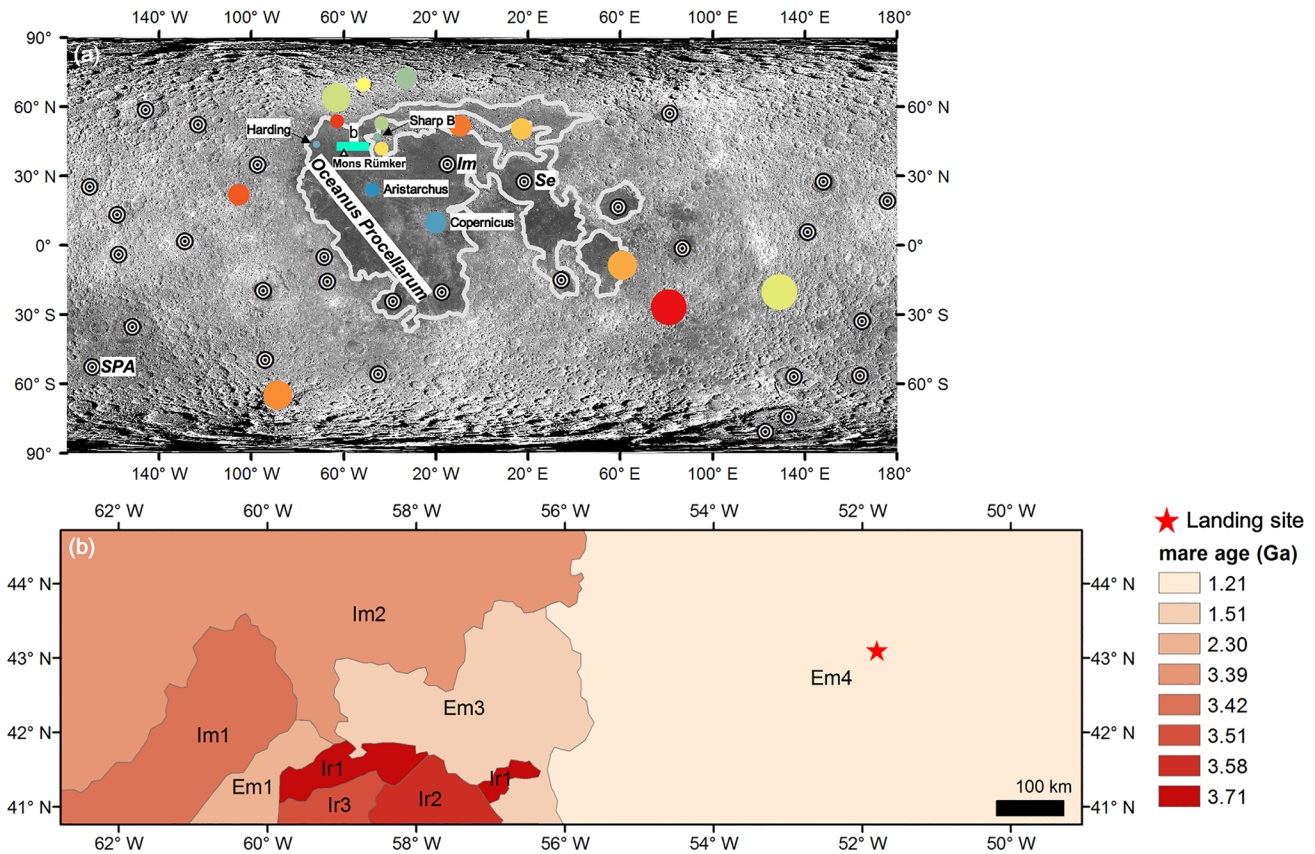
Figure 1. (a) The geologic context of the CE-5 landing region (the cyan square inside the maria). The colored circles present the impact craters that likely have affected the material composition of the landing region, where the redder color indicates the older age and the greater size suggests the larger diameter. We expect four impacts (Sharp B, Harding, Copernicus, and Aristarchus) have significantly altered the material composition of the landing surface. Concentric symbols mark the basin center. We expect SPA, Imbrium and Serenitatis basin are the main contributors of the nonmare materials in the CE-5 samples. The base map is a LRO WAC mosaic (Robinson et al., 2010). (b) The mare units of the landing region (after Qian et al. 2018).

a sequence of impact events was generated using the Monte Carlo method. Impact events of different sizes were randomly distributed over the Moon in chronological sequence. For each impact, both the excavation process and ejecta deposition were considered. The excavated material was emplaced outside the crater cavity as ejecta layers. For the ejecta that are deposited near the crater rim, the thickness decreases with distance from the crater center (r): $\delta(r) = Ar^{-3}$, where A is a constant, and it was calculated by taking the total ejecta volume to be the excavation volume. Due to the importance of distal ejecta (Huang et al., 2017; Liu, Michael, Zuschneid, et al., 2020), the power law was extrapolated to greater distances. The high-velocity ejecta was expected to mix with local material during emplacement. The degree of mixing was quantified using a mixing ratio of local material to ejecta, $\mu = 0.0183r^{0.87}$; when μ is larger than 5.0: $\mu' = \mu / 2 + 2.5$ (Oberbeck et al., 1975; Petro & Pieters, 2006). One million points that are uniformly distributed over a sphere with the Moon's radius recorded the volume of different components with depth. Each point was related to a certain area of $\sim 5 \times 5$ km^2. A more detailed description of the model is provided in Liu, Michael, Wünnemann, et al. (2020).

The CE-5 landing region is located on a young mare surface. For craters forming on the highlands, only large craters whose distal ejecta are more likely to reach the remote areas may deposit ejecta at the landing region. Also, only larger craters with a diameter at least 10 times the local mare thickness can excavate materials from underneath the mare deposits to the surface. Thus, the minimum crater diameter is considered in this study and is taken to be 5 km to match the spatial resolution of the global model (Liu, Michael, Wünnemann, et al., 2020). Specific impact craters (Figure 1 and Table S1) whose ejecta were proposed to affect the landing surface are added individually into the model. The diffusion of their ejecta through impact

gardening is simulated. Except for the listed impacts, the positions of other craters are randomly generated over the Moon.

Impact-generated melt records the occurrence time for the formation of a given basin (Schärer, 1998). With the determined crater density over the provenance surface, the dating of basin-sourced melt contained in samples can provide pinpoint references for creating a chronology system (Hiesinger et al., 2011; Neukum & Ivanov, 1994; Neukum et al., 2001; Stöffler & Ryder, 2001; Wilhelms, 1987). To predict the amount of basin melt that could be found in the CE-5 samples and its plausible composition, we adopt the composition of the lunar surface prior to the emplacement of mare materials from the estimates of Liu, Michael, Wünnemann et al. (2020). In their model, the total generated melt of each crater with the age of impact occurrence time was calculated according to its crater size (Cintala & Grieve, 1998). The subsequent impacts reset the age of the existing melt and altered its spatial distribution. The model simulated was slightly earlier than the formation of the South Pole-Aitken (SPA) basin, and involved 30 basins-forming events (Table S2). The estimated melt composition for middle to last basin-forming events was calibrated with Apollo and Luna samples and the predicted abundant old basin melt has been frequently detected recently (e.g., Vanderliek et al., 2018).

3.2. Mare Filling

The mare filling process was embedded into the model to investigate the material exchange between the mare and highland regions before to predict the mare concentration over the entire mare region and at the Apollo and Luna landing site. The results provided a good match with the average mare fraction of the returned soil samples (Liu, Michael, Zuschneid, et al., 2020). Because of the uncertainty of both mare thickness and volcanic flux, simulations with various scenarios of volcanic filling were performed. It was found that the key factors affecting the mare/nonmare composition of surface material are the total mare thickness and the occurrence time of the latest mare filling. The former influences the abundance of nonmare component that was vertically excavated from beneath the mare deposits. The later determines the composition of nonmare component that was laterally transported from the highlands. Simulations where the mare materials were rapidly emplaced and where the filling was more gradual were also considered. The results showed that for the given total mare thickness, no distinct difference of the material composition is observed. For simplicity, we here assume the mare material is rapidly emplaced on the mare regions.

In this study, the model starts slightly earlier than 3.72 Ga, the time for the earliest detectable volcanism over Oceanus Procellarum (Hiesinger et al., 2003). When the model time (t) is equal to 3.72 Ga, the whole Oceanus Procellarum region is filled with the mare material with a thickness of 500 m (De Hon, 1979; Liu, Michael, Zuschneid, et al., 2020), the representatively lower limit of total mare thickness including deep-buried old mare deposits. Only inside the landing region are the younger mare effusion events considered. The thickness, occurrence time, and coverage of late events are all adopted from previous results (Figure 1b). Once t is equal to the age of any mare units of the landing region, the unit surface with this age will be filled with mare components with a proposed thickness (Ir-aged and Imbrian-aged units are 700 m; Eratosthenian units are 100 m). Note that there are still uncertainties on the estimates of mare thickness. For example, based on the morphology of partially buried craters the overall mare thickness of the lunar nearside was estimated to be 500 m (De Hon, 1974, 1979; De Hon & Waskom, 1976) which is thinner than that is inspired by the identified buried impact craters from gravity data (Evans et al., 2016). Within the CE-5 landing region, the estimated mare thickness of the surface Em4 unit is ~100 m from Qian et al. (2018), thinner than 30–60 m from Hiesinger et al. (2003). To investigate the influence of mare thickness on the material composition of the landing surface, simulations with the half (Ir-aged and Imbrian-aged units are 350 m; Eratosthenian units are 50 m) and double thickness (Ir-aged and Imbrian-aged units are 1,400 m; Eratosthenian units are 200 m) of the mare deposit are performed.

In this way, our previous model is refocused on the evolution of material composition over the CE-5 region. While the impact events happen in chronological sequence, the mare filling events over the defined area at a certain time occur.
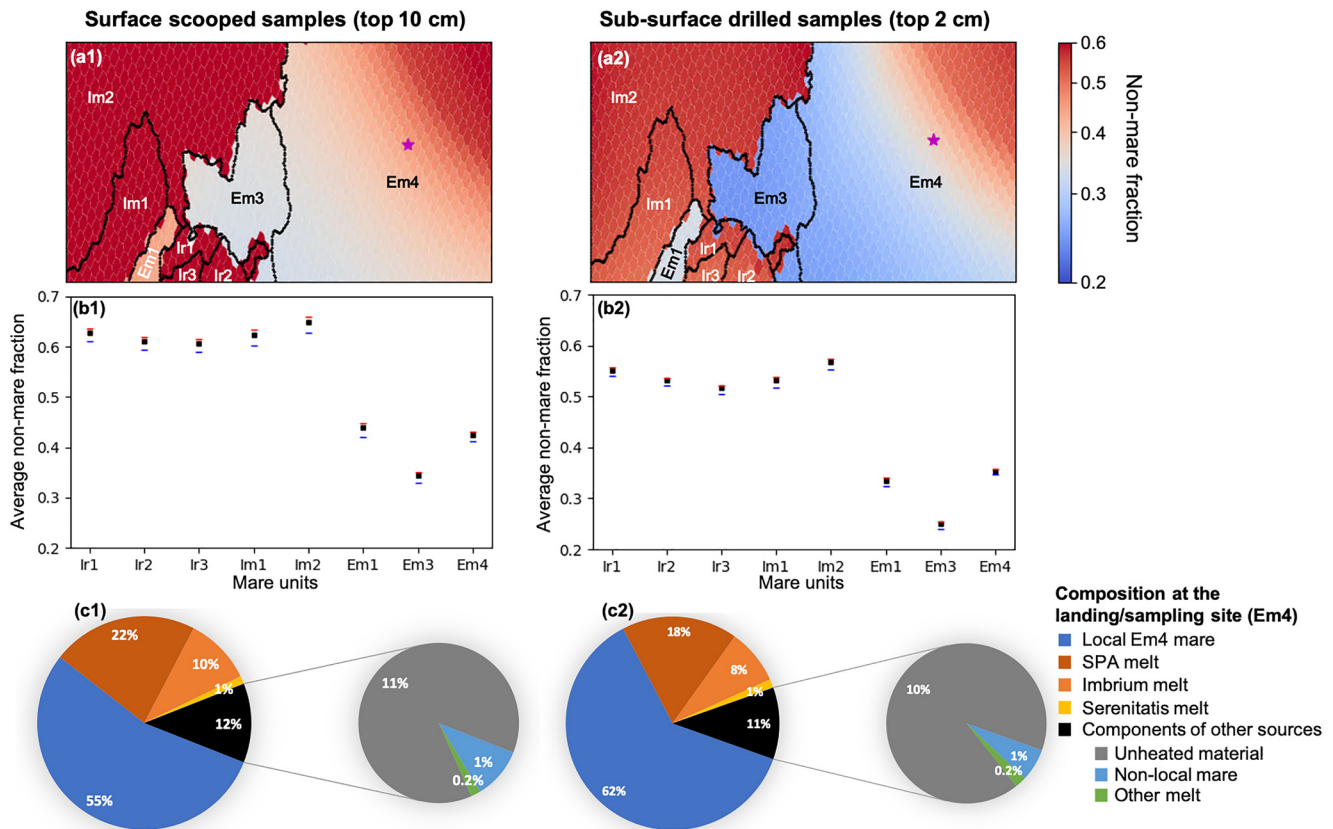
Figure 2. Predicted material composition of surface (left) and sub-surface (right) materials. (a1 and a2) The distribution of nonmare component over the landing region. The star indicates the landing site. (b1 and b2) The average nonmare mixture among the mare units. Squares are the estimate of (a1 and a2), and red and blue data are the estimates based on the simulations with thinner (×0.5, Ir-aged and Imbrian-aged units are 350 m; Eratosthenian units are 50 m) and thicker (×2.0, Ir-aged and Imbrian-aged units are 1,400 m; Eratosthenian units are 200 m) mare deposits, respectively. (c1 and c2) Material composition at the sampling site.

4. Results and Discussions

In line with two types of CE-5 sampling strategy, we estimate the composition of both the surface (top 10 cm) and sub-surface (top 2 m) material. The predicted material composition of different depths provides quantitative references for the analysis of CE-5 samples collected from the surface and in the drilling core (∼2 m; Qian et al., 2020).

4.1. Material Composition over the Landing Region

The distance of the CE-5 landing site to the closest northern and eastern highlands is ∼100 and ∼300 km, respectively. The proximity to the highlands increases the likelihood of a significant laterally transported nonmare component (Huang et al., 2017; Liu, Michael, Zuschneid, et al., 2020). Our results show that the big picture of the surface (top 10 cm) and sub-surface (top 2 m) material composition displays similar features (Figures 2a1 and 2a2): the whole landing region contain some nonmare components. Older surfaces tend to contain more nonmare material. Due to being closer to the highlands, the average nonmare fraction of the Im2 surface is higher than the oldest Ir1 unit (Figures 2b1 and 2b2). In the Em4 unit, the northeastern part that is nearer to the highlands, possesses a distinctly higher nonmare mixture than the remainder. It leads to the average nonmare abundance of the youngest Em4 being higher than the older Eratosthenian mare units (Em1, Em3) (Figures 2a1 and 2a2). Besides, since the nonmare component that was transported to the landing region after the filling of the youngest mare material gathers in the topmost surface, the

nonmare concentration of surface material (35%–65%) is generally greater than that of sub-surface material (25%–60%).

Simulations considering both thinner (×0.5) and thicker (×2.0) mare deposits present comparable results. The difference of the average nonmare fraction is smaller than ~0.02 and ~0.01 in the top 10 cm and 2 m, respectively (Figures 2b1 and 2b2). Given the age of mare units, the abundance of laterally transported nonmare component is the same. The difference is caused by the varying concentration of the re-excavated nonmare material that was buried under the mare deposits. However, due to the predominance of mare components and the small size of craters (<2 km; Table S3), the re-excavated nonmare component from beneath the mare deposits is rare that cannot significantly yield the difference of nonmare fraction.

4.2. Material Composition of the Landing/Sampling Site (Em4)

We predict the average composition of surface and sub-surface material at the landing/sampling site (Figures 2c1 and 2c2). The surface material contains ~55% mare material, smaller than that of the sub-surface material (~60%). Except for the mare concentration, the bulk fraction of the other components in the surface and sub-surface is comparable: Impact melt accounts for a large proportion of nonmare components. The unheated components are ~10% of the total materials.

Our model does not consider the gardening of smaller and secondary impacts. If the impact gardening depth is shallower than the sampling depth, this process would thoroughly mix the different components; otherwise, more deep-seated components would be added to the near-surface. Given the surface age of 1.21 Ga (Em4), the deepest depth overturned at least one time is ~1.5 m (Costello et al., 2020), which falls in between the surface (10 cm) and sub-surface (2 m) sampling depth. For the surface samples, since their material composition differs slightly when compared with materials in the greater depth on the mare abundance (Figures 2c1 and 2c2), the gardening of smaller craters may slightly increase the mare concentration. For the sub-surface material, this process would not change the bulk composition, but in the drilling core, we may see a more homogeneous composition in the upper part and the more mare component in the deeper part. In addition, the average regolith thickness of the landing region was estimated to be ~7 m (Qian et al., 2020). If the different components are extensively mixed in the regolith, we cannot see the aforementioned distinct layering.

4.2.1. Mare Components

The mare components include the local material from the Em4 unit and nonlocal mare components that were entrained in the ejecta of craters outside the Em4 unit and deposited at the landing site. To estimate the nonlocal mare abundance, we traced separately the diffusion of the mare components other than Em4 (Figure 1). Our results show that the local Em4 mare component is predominant among all the mare materials and the nonlocal mare components are only ~1% (Figures 2c1 and 2c2). Due to the late mare filling of the Em4 unit, all the early transported nonlocal mare components should be buried. Impacts occurring after the Em4 emplacement may have transported some nonlocal mare material to the landing site. However, as the most late-forming craters over the landing region are smaller than 2 km (Table S3), the nonmare component fraction excavated from beneath the mare layer and deposited at the landing site is small. Besides, the distance from the landing site, even to the boundary of the nearest Em3 unit, is >80 km. If a 2-km-crater occurred on the boundary and some of its excavated material reached the landing site, the quantity of deposited material would also be small because a very little amount of ejected material can be transported so far.

4.2.2. Basin-Sourced Impact Melt

Once the basin melt was generated, it could be dispersed over a broader area by nearby large impacts and it could also be deeply buried by the thick ejecta of subsequent impacts. Some of the melt can be re-heated generating melt with younger ages (Fernandes et al., 2013; Liu, Michael, Engelmann, et al., 2019; Liu, Michael, Wünnemann, et al., 2020; Michael et al., 2018). For differently aged impact melt, it is difficult to distinguish whether it is derived from large basins or smaller craters, which yields the uncertainty of lunar geochronology system (Hiesinger et al., 2011; Neukum et al., 2001; Neukum & Ivanov, 1994; Stöffler & Ryder, 2001; Wilhelms, 1987). We predicted melt composition to explain the possible provenance of impact
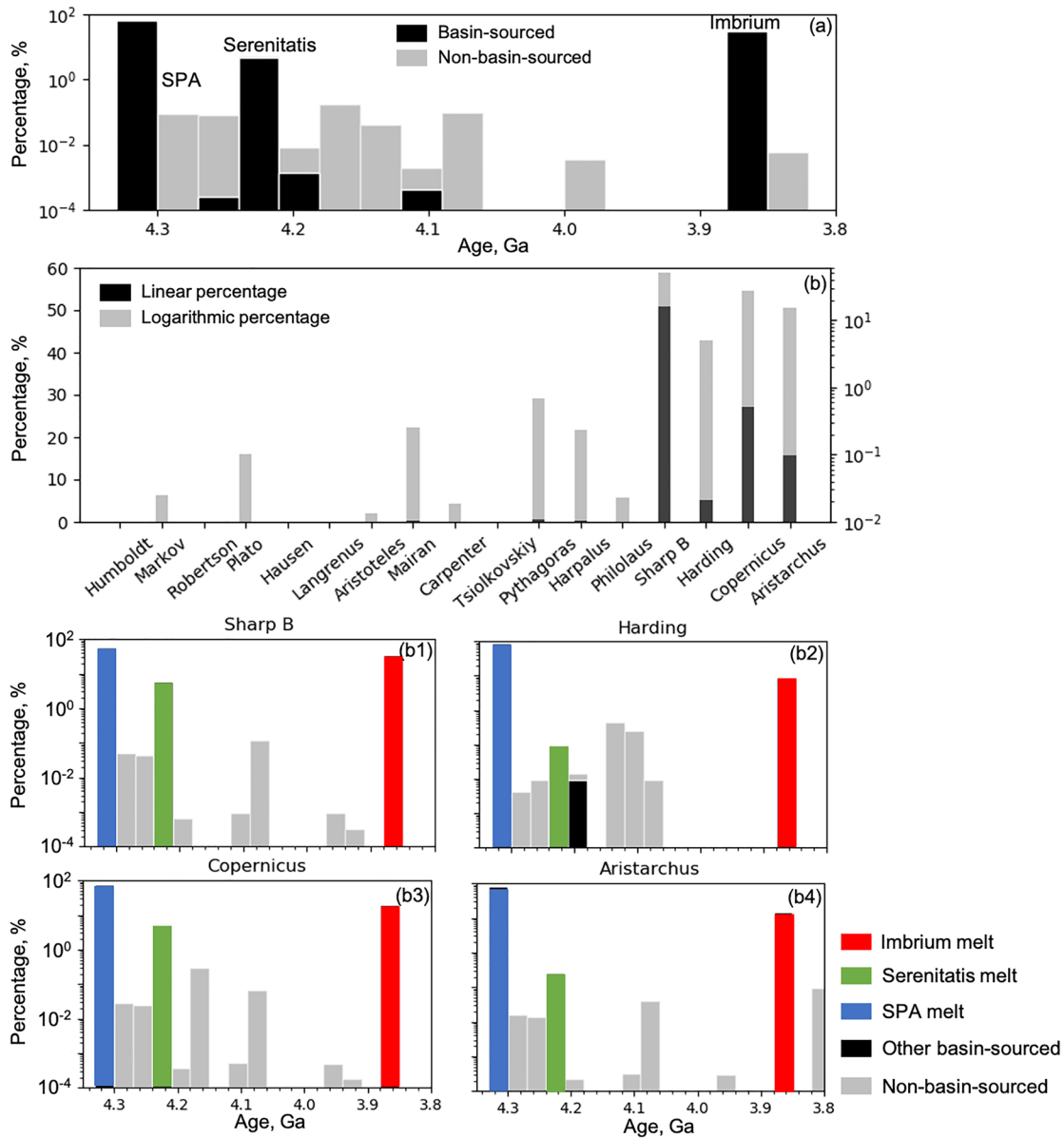
Figure 3. Nonmare composition in the top two meters. (a) Impact melt composition among all the predicted melt materials. Three major contributors (SPA, Serenitatis, and Imbrium) are highlighted. (b) The relative abundance of the ejecta from the listed impacts. Panels (b1–b4) are the melt composition of the ejecta of the four major contributors (Sharp B, Harding, Copernicus, and Aristarchus), the location of which is presented in Figure 1a.

melt in the CE-5 sub-surface samples (Figure 3a; the surface samples possess the similar nonmare composition, Figures 2c1 and 2c2).

Our models present abundant melt of various basin-origin. Being approaching the young Imbrium basin (Figure 1), the sampling site would possess Imbrium melt. Here, we predict that the collected CE-5 sample suit may contain abundant melt from Imbrium basin, similar to Apollo and luna samples. These material contained in the CE-5 sample suite can be used to improve our knowledge of Imbrium formation (Snape et al., 2016). Although the Serenitatis basin is relatively far away, the late-forming Imbrium basin could have excavated some Serenitatis melt and dispersed them to the landing site (Liu, Michael, Wünnemann, et al., 2020). The SPA basin, ~2500 km in diameter, has produced a huge volume of impact melt likely covering the global surface. As SPA was formed very early (~4.3 Ga), its melt was redistributed by impact gardening several times resulting in a complicated spatial distribution pattern. Our results show that there

could still be some SPA melt (∼50% among all the nonmare material, Figure 3a) present at the landing region. However, the steady comminution by the long-lasting impact gardening very likely has led to too small melt samples being present at the landing site that can be dated using conventional isotopic methods (e.g., Cohen et al., 2001; Liu, Michael, Engelmann, et al., 2019; Liu, Michael, Wünnemann, et al., 2020; Maurer et al., 1978; Michael et al., 2018). Besides, the estimated SPA component should be regarded as an extreme limit, since its ejecta distribution was simulated as that of the smaller craters, but there are numerous uncertainties regarding the SPA formation (Petro & Pieters, 2008). The concentration of other basin-sourced melts is small (Figure 3a).

4.2.3. Basin-Sourced Melt in Ejecta of the Listed Craters

Secondary crater clusters, the evidence of distal ejecta of large craters, are present in the landing region (Qian et al., 2018). They indicate the nonnegligible influence of their source impacts on the material composition at the landing site. Given the formation sequence of the listed impact events (Table S1), we calculate the abundance of their emplaced ejecta that could still remain on the landing surface after the subsequent impact mixing and mare filling. Figure 3b presents the relative contribution of ejecta from the listed impacts on the landing site, from which we can find crater Sharp B, Harding, Copernicus, and Aristarchus are the major contributors of ejecta at the landing site. These craters are formed after the filling of Em4 unit and their ejecta can be well-preserved. The earlier crater ejecta at the landing site are buried. With the subsequent impact gardening some of the buried components could be re-excavated. However, our results show that the volume of these re-excavated components is small, and the re-excavated older ejecta is <2% among the total ejecta of all the listed impacts.

Due to the long-term impact mixing, the distribution of basin-sourced melt is spatially different, and hence the excavated material of the listed impacts consists of various melt compositions. Assuming the materials are thoroughly mixed during the excavation process, and the ejecta composition at various distances from the crater center is the same, the composition of basin-sourced melt in the distal ejecta that later emplace on the landing surface can be calculated. Figures 3b1–3b4 present the melt composition of the major contributors from Sharp B, Harding, Copernicus, and Aristarchus crater. All their ejecta contain abundant melt from the SPA and Imbrium basin. The mixture of Serenitatis melt in the ejecta of Sharp B and Copernicus crater is greater than the other two craters.

Note that, in our model, we assume the distal ejecta is uniformly and continuously distributed, whereas their emplacement is more likely to be patchy (Melosh, 1989). Places superposed by the patchy distal ejecta locally have thicker transported material than their background. Therefore, there would be an uncertainty about the absolute volume of distal ejecta, but as long as the collected samples contain these distal ejecta, the relative abundance of differently basin-sourced components should be comparable with our prediction.

5. Conclusions

New samples from the young mare surface have become available through CE-5 sample-return mission. To investigate the mare/nonmare composition of these samples, we applied a spatially resolved model to trace the diffusion of different components at the landing region, in which both the impact gardening and the mare filling are involved. We expect that the major difference in composition between the surface scooped (10 cm) and the drilled (2 m) samples will be the concentration of the local mare material, where the surface samples contain ∼55%, less than the sub-surface scooped samples (∼60%). A significant amount of nonmare material should be present in the samples of different depths and the composition is similar. The SPA, Serenitatis, and Imbrium melt could account for ∼70% among all the nonmare components, and the Imbrium melt accounts for ∼25% among all the impact melt. The predicted abundant Imbrium melt in the CE-5 samples provides us an opportunity to verify our knowledge of its formation time. Despite having a large volume, the older SPA melt is likely difficult to identify because of its small particle size caused by the extensive comminution. Among the mare components, very few nonlocal mare components can be found indicating that the separate mare emplacement is difficult to find in the samples. The ejecta of the Sharp B, Harding, Copernicus, and Aristarchus crater may have significantly altered the material composition at the landing site. Among these four craters, the Copernicus and Sharp B crater would be the carrier of the

Serenitatis melt, and all of them could excavate abundant pre-deposited melt from the SPA and Imbrium basin to the landing site.

Data Availability Statement

Data underlie the figures are available at Liu et al. (2021) https://doi.org/10.35003/IOFFGV.

References

Beaty, D. W., & Albee, A. L. (1978). Comparative petrology and possible genetic relations among the Apollo 11 basalts. *Lunar and Planetary Science Conference Proceedings*, *9*, 359–463.

Bottke, W. F., & Norman, M. D. (2017). The late heavy bombardment. *Annual Review of Earth and Planetary Sciences*, *45*(1), 619–647. https://doi.org/10.1146/annurev-earth-063016-020131

Cintala, M. J., & Grieve, R. A. F. (1998). Scaling impact melting and crater dimensions: Implications for the lunar cratering record. *Meteoritics and Planetary Science*, *33*(4), 889–912. https://doi.org/10.1111/j.1945-5100.1998.tb01695.x

Cohen, B. A., Snyder, G. A., Hall, C. M., Taylor, L. A., & Nazarov, M. A. (2001). Argon-40-argon-39 chronology and petrogenesis along the eastern limb of the Moon from Luna 16, 20 and 24 samples. *Meteoritics & Planetary Science*, *36*(10), 1345–1366. https://doi.org/10.1111/j.1945-5100.2001.tb01829.x

Costello, E. S., Ghent, R. R., Hirabayashi, M., & Lucey, P. G. (2020). Impact gardening as a constraint on the age, source, and evolution of ice on Mercury and the Moon. *Journal of Geophysical Research: Planets*, *125*(3), e2019JE006172. https://doi.org/10.1029/2019je006172

De Hon, R. A. (1974). Thickness of mare material in the Tranquillitatis and Nectaris basins. *Lunar and Planetary Science Conference Proceedings*, *5*, 53–59.

De Hon, R. A. (1979). Thickness of western mare basalts. *Proceedings of the 10th Lunar and Planetary Science Conference*, 2935–2955.

De Hon, R. A., & Waskom, J. D. (1976). Geologic structure of the eastern mare basins. *Lunar and Planetary Science Conference Proceedings*, *3*, 2729–2746.

Evans, A. J., Soderblom, J. M., Andrews-Hanna, J. C., Solomon, S. C., & Zuber, M. T. (2016). Identification of buried lunar impact craters from GRAIL data and implications for the nearside maria. *Geophysical Research Letters*, *43*(6), 2445–2455. https://doi.org/10.1002/2015gl067394

Fernandes, V. A., Fritz, J., Weiss, B. P., Garrick-Bethell, I., & Shuster, D. L. (2013). The bombardment history of the Moon as recorded by 40 Ar-39 Ar chronology. *Meteorit Planet Science*, *48*(2), 241–269. https://doi.org/10.1111/maps.12054

Hiesinger, H., & Head, J. W. (2006). New views of lunar geoscience: An introduction and overview. *Reviews in Mineralogy and Geochemistry*, *60*(1), 1–81. https://doi.org/10.2138/rmg.2006.60.1. https://doi.org/10.2138/rmg.2006.60.1

Hiesinger, H., Head, J. W., Wolf, U., Jaumann, R., & Neukum, G. (2003). Ages and stratigraphy of mare basalts in Oceanus Procellarum, Mare Nubium, Mare Cognitum, and Mare Insularum. *Journal of Geophysical Research: Planets*, *108*(E7), 5065. https://doi.org/10.1029/2002je001985

Hiesinger, H., Head, J. W., Wolf, U., Jaumann, R., & Neukum, G. (2011). Ages and stratigraphy of lunar mare basalts: A synthesis. *Recent Advances and Current Research Issues in Lunar Stratigraphy*, *477*, 1–51. https://doi.org/10.1130/2011.2477(01)

Huang, Y., Minton, D. A., Masatoshi, H., Elliott, J. R., Richardson, J. E., Fassett, C. I., & Zellner, N. E. B. (2017). Heterogeneous impact transport on the Moon. *Journal of Geophysical Research: Planets*, *122*, 1–23. https://doi.org/10.1002/2016je005160

Korotev, R. L., & Jolliff, B. L. (2001). The curious case of the lunar magnesian granulitic breccias. *Lunar and Planetary Science Conference*, 1455.

Liu, T., Michael, G., Engelmann, J., Wünnemann, K., & Oberst, J. (2019). Regolith mixing by impacts: Lateral diffusion of basin melt. *Icarus*, *321*(0019–1035), 691–704. https://doi.org/10.1016/j.icarus.2018.12.026

Liu, T., Michael, G., Wünnemann, K., Becker, H., & Oberst, J. (2020). Lunar megaregolith mixing by impacts: Spatial diffusion of basin melt and its implications for sample interpretation. *Icarus*, *339*. https://doi.org/10.1016/j.icarus.2019.113609

Liu, T., Michael, G., Zuschneid, W., Wünnemann, K., & Oberst, J. (2020). Lunar megaregolith mixing by impacts: Evaluation of the non-mare component of mare soils. *Icarus*, *358*(1–3), 114206. https://doi.org/10.1016/j.icarus.2020.114206

Maurer, P., Eberhardt, P., Geiss, J., Grögler, N., Stettler, A., Brown, G. M., et al. (1978). Pre-Imbrian craters and basins: ages, compositions and excavation depths of Apollo 16 breccias. *Geochimica et Cosmochimica Acta*, *42*(11), 1687–1720. https://doi.org/10.1016/0016-7037(78)90257-0

Melosh, H. J. (1989). *Impact cratering: A geologic process*. Oxford University.

Michael, G., Basilevsky, A., & Neukum, G. (2018). On the history of the early meteoritic bombardment of the Moon: Was there a terminal lunar cataclysm? *Icarus*, *302*, 80–103. https://doi.org/10.1016/j.icarus.2017.10.046

Neukum, G. (1983). Meteoritenbombardement und Datierung Planetarer Oberflaechen. *Habilitation dissertation for faculty membership* (pp. 1–186). Univ. of Munich.

Neukum, G., & Ivanov, B. A. (1994). Crater size distributions and impact probabilities on Earth from lunar, terrestrial-planet, and asteroid cratering data. *Hazards Due to Comets and Asteroids*, *359*(1), 359–416.

Neukum, G., Ivanov, B. A., & Hartmann, W. K. (2001). Cratering records in the inner solar system in relation to the lunar reference system. *Space Science Reviews*, *96*(1–4), 55–86. https://doi.org/10.1007/978-94-017-1035-0_3

Norman, M. D., & Nemchin, A. A. (2014). A 4.2 billion year old impact basin on the Moon: U-Pb dating of zirconolite and apatite in lunar melt rock 67955. *Earth and Planetary Science Letters*, *388*, 387–398. https://doi.org/10.1016/j.epsl.2013.11.040

Norman, M. D., Taylor, L. A., Shih, C.-Y., & Nyquist, L. E. (2016). Crystal accumulation in a 4.2 Ga lunar impact melt. *Geochimica et Cosmochimica Acta*, *172*, 410–429. https://doi.org/10.1016/j.gca.2015.09.021

Oberbeck, V. R., Hörz, F., Morrison, R. H., Quaide, W. L., & Gault, D. E. (1975). On the origin of the lunar smooth-plains. *The Moon*, *12*(1), 19–54. https://doi.org/10.1007/bf02626332

Petro, N. E., & Pieters, C. M. (2006). Modeling the provenance of the Apollo 16 regolith. *Journal of Geophysical Research*, *111*(E9), E09005. https://doi.org/10.1029/2005je002559

Petro, N. E., & Pieters, C. M. (2008). The lunar-wide effects of basin ejecta distribution on the early megaregolith. *Meteoritics & Planetary Science*, *43*(9), 1517–1529. https://doi.org/10.1111/j.1945-5100.2008.tb01025.x

Qian, Y. Q., Xiao, L., Zhao, S. Y., Zhao, J. N., Huang, J., Flahaut, J., et al. (2018). Geology and Scientific Significance of the Rümker Region in Northern Oceanus Procellarum: China's Chang'E-5 Landing Region. *Journal of Geophysical Research: Planets*, *123*(6), 1407–1430. https://doi.org/10.1029/2018je005595

Qian, Y., Xiao, L., Yin, S., Zhang, M., Zhao, S., Pang, Y., et al. (2020). The regolith properties of the Chang'e-5 landing region and the ground drilling experiments using lunar regolith simulants. *Icarus*, *337*, 113508. https://doi.org/10.1016/j.icarus.2019.113508

Rhodes, J. M., Rodgers, K. V., Shih, C., Bansal, B. M., & Nyquist (1974). The relationships between geology and soil chemistry at the Apollo 17 landing site. *Proceedings of 5th Lunar Science Conference*, *5*(2), 1097–1117.

Robinson, M. S., Brylow, S. M., Tschimmel, M., Humm, D., Lawrence, S. J., Thomas, P. C., et al. (2010). Lunar reconnaissance orbiter camera (LROC) instrument overview. *Space Science Reviews*, *150*(1–4), 81–124. https://doi.org/10.1007/978-1-4419-6391-8_6

Schärer, U. (1998). Dating of Impact Events. In D. Benest, & C. Froeschlé (Eds.), *Impacts on Earth* (pp. 157–183). Springer Berlin Heidelberg.

Snape, J. F., Nemchin, A. A., Grange, M. L., Bellucci, J. J., Thiessen, F., & Whitehouse, M. J. (2016). Phosphate ages in Apollo 14 breccias: Resolving multiple impact events with high precision U-Pb SIMS analyses. *Geochimica et Cosmochimica Acta*, *174*, 13–29. https://doi.org/10.1016/j.gca.2015.11.005

Spudis, P. D., & Ryder, G. (1981). Apollo 17 impact melts and their relation to the Serenitatis basin. *Multi-Ring Basins: Formation and Evolution*, 133–148.

Stöffler, D. (2006). Cratering history and lunar chronology. *Reviews in Mineralogy and Geochemistry*, *60*(1), 519–596. https://doi.org/10.2138/rmg.2006.60.05

Stöffler, D., & Ryder, G. (2001). Stratigraphy and isotope ages of lunar geologic units: Chronological standard for the inner solar system. In R. Kallenbach, J. Geiss, W. K. Hartmann (Eds.), *Chronology and evolution of Mars* (pp. 9–54). Springer Netherlands.

Vanderliek, D. M., Becker, H., & Rocholl, A. (2018). In situ U-Pb dating of lunar breccia 15455: Impact resetting and growth of zircons at 4.2 Ga. *Lunar and Planetary Science Conference*, *49*, 1931.

Vaniman, D., Dietrich, J., Taylor, G. J., & Heiken, G. (1991). Exploration, samples, and recent concepts of the Moon. In G. H. Heiken, D. T. Vaniman, & B. M. French (Eds.), *Lunar source-book: A user's guide to the Moon* (pp. 5–26). Cambridge University Press.

Wilhelms, D. E. The geologic history of the Moon. *U.S. Geological Survey Professional Paper* (Vol. *1348*). https://doi.org/10.1007/s13398-014-0173-7.2

Wu, B., Huang, J., Li, Y., Wang, Y., & Peng, J. (2018). Rock abundance and crater density in the candidate chang'E-5 landing region on the Moon. *Journal of Geophysical Research: Planets*, *123*(12), 3256–3272. https://doi.org/10.1029/2018je005820

Xie, M., Xiao, Z., Zhang, X., & Xu, A. (2020). The provenance of regolith at the chang'e-5 candidate landing region. *Journal of Geophysical Research: Planets*, *125*(5), e2019JE006112. https://doi.org/10.1029/2019je006112

Zhao, J., Xiao, L., Qiao, L., Glotch, T. D., & Huang, Q. (2017). The Mons Rümker volcanic complex of the Moon: A candidate landing site for the Chang'E-5 mission. *Journal of Geophysical Research: Planets*, *122*(7), 1419–1442. https://doi.org/10.1002/2016je005247

Zou, Y. L., & Li, W. (2017). Scientific visions of lunar research-station from China. *Lunar and Planetary Science Conference*, 1730.